JCI insight

Reactive astrocyte-driven epileptogenesis is induced by microglia initially activated following status epilepticus

Fumikazu Sano, Eiji Shigetomi, Youichi Shinozaki, Haruka Tsuzukiyama, Kozo Saito, Katsuhiko Mikoshiba, Hiroshi Horiuchi, Dennis Lawrence Cheung, Junichi Nabekura, Kanji Sugita, Masao Aihara, Schuichi Koizumi

JCI Insight. 2021. https://doi.org/10.1172/jci.insight.135391.

Research In-Press Preview Neuroscience

Graphical abstract

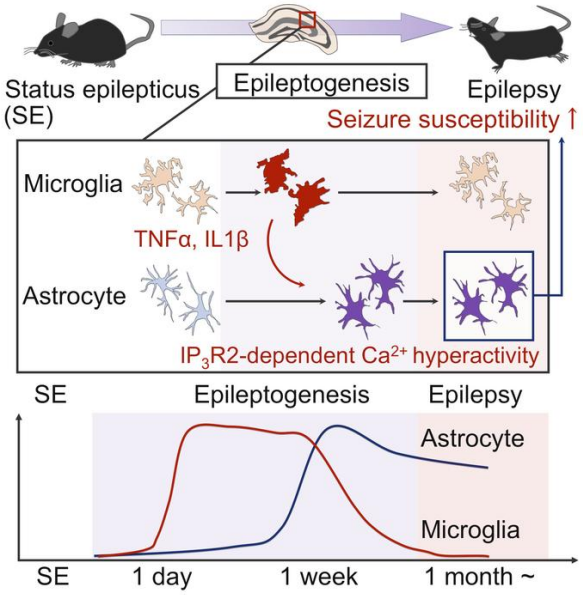

Find the latest version:

https://jci.me/135391/pdf

Reactive astrocyte-driven epileptogenesis is induced by microglia initially activated following status epilepticus

Fumikazu Sano[1,2,3], Eiji Shigetomi[1,3], Youichi Shinozaki[1,3], Haruka Tsuzukiyama[1], Kozo Saito[1,3,4], Katsuhiko Mikoshiba[5], Hiroshi Horiuchi [6], Dennis Lawrence Cheung[6], Junichi Nabekura[6], Kanji Sugita[2], Masao Aihara[2], Schuichi Koizumi[1,3]*

1 Department of Neuropharmacology, Interdisciplinary Graduate School of Medicine, University of Yamanashi, Yamanashi, Japan,

2 Department of Pediatrics, Faculty of Medicine, University of Yamanashi, Yamanashi, Japan,

3 GLIA Center, Interdisciplinary Graduate School of Medicine, University of Yamanashi, Yamanashi, Japan,

4 Department of Neurology, Graduate School of Medical Science, Kyoto Prefectural University of Medicine, Kyoto, Japan,

5 Shanghai Institute for Advanced Immunochemical Studies, ShanghaiTech University, Shanghai, China

6 Division of Homeostatic Development, National Institute for Physiological Sciences, Okazaki, Japan

*Corresponding Author: Schuichi Koizumi, University of Yamanashi, 1110 Chuo, Yamanashi, 409-3898, Japan.

Phone: +81-55-273- 9503; Email: skoizumi@yamanashi.ac.jp.

Conflicts of interest: The authors have declared that no conflict of interest exists.

Abstract

Extensive activation of glial cells during a latent period has been well documented in various animal models of epilepsy. However, it remains unclear whether activated glial cells contribute to epileptogenesis; i.e., the chronically persistent process leading to epilepsy. Particularly, it is not clear whether inter-glial communication between different types of glial cells contributes to epileptogenesis, as past literature mainly focused on one type of glial cell. Here, we show that temporally distinct activation profiles of microglia and astrocytes collaboratively contribute to epileptogenesis in a drug-induced status epilepticus model. We found that reactive microglia appeared first, followed by reactive astrocytes and increased susceptibility to seizures. Reactive astrocytes exhibited larger Ca^{2+} signals mediated by IP_3R2, whereas deletion of this type of Ca^{2+} signaling reduced seizure susceptibility after status epilepticus. Immediate, but not late, pharmacological inhibition of microglial activation prevented subsequent reactive astrocytes, aberrant astrocyte Ca^{2+} signaling, and the enhanced seizure susceptibility. These findings indicate that the sequential activation of glial cells constitutes a cause of epileptogenesis after status epilepticus. Thus, our findings suggest that the therapeutic target to

prevent epilepsy after status epilepticus should be shifted from microglia (early phase) to astrocytes (late phase).

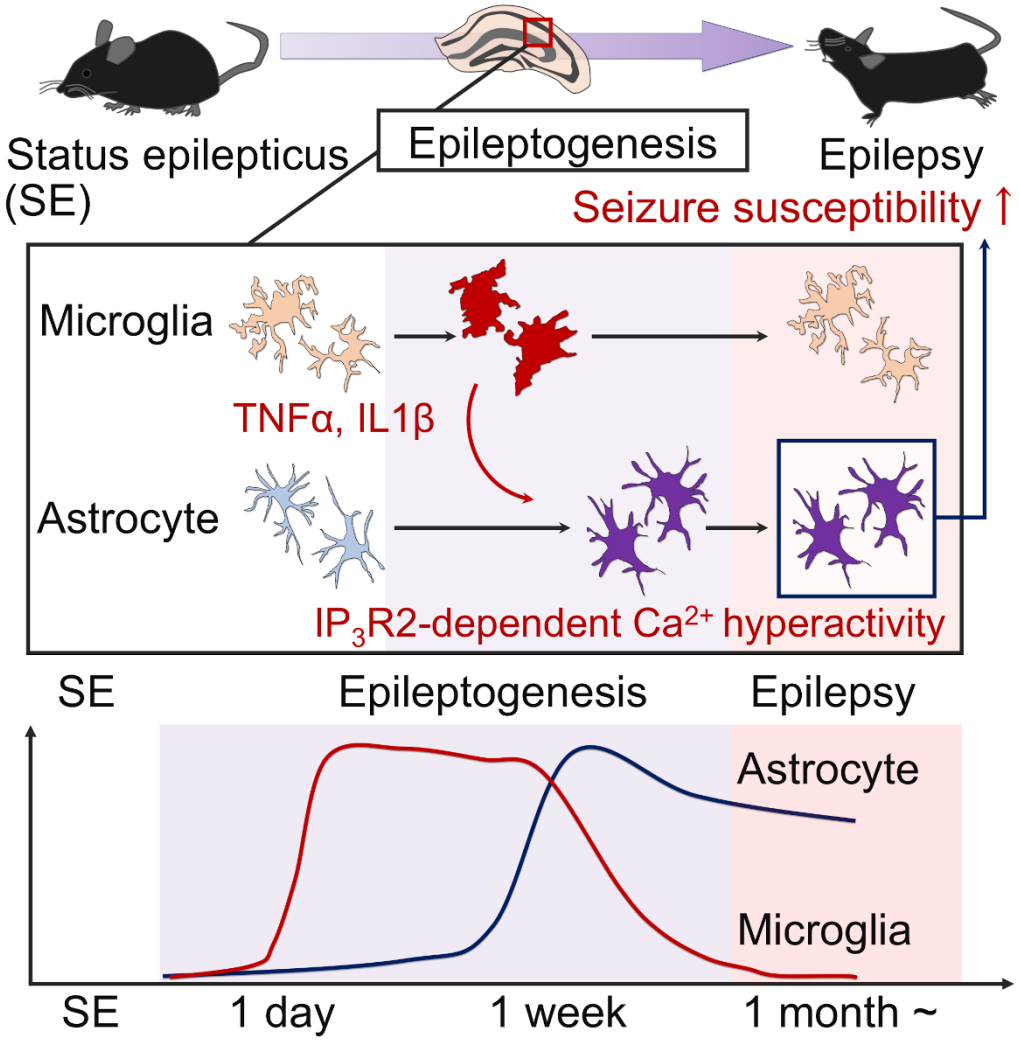

Introduction

Epileptogenesis; i.e., the process leading to epilepsy, is a common sequel of brain insults such as brain injury, cerebrovascular disease, or status epilepticus (SE) (1,2). Such brain insults are typically followed by a latent period, during which the brain undergoes a cascade of morphological and functional changes over month to years prior to the onset of chronic epilepsy (3,4). Extensive activation of glial cells, including microglia and astrocytes, has been well documented during this latent period in various animal models of epilepsy (5–7). Although the association of pathology with reactive glial cells is widely recognized, it is unclear whether such microglial and astrocytic activation constitutes primary causes of epilepsy or rather represents the results of repeated seizures. Moreover, the potential for these reactive glial cells to comprise candidates for epileptogenesis raises the further mechanistic question regarding whether activated glial cells might contribute to epileptogenesis independently or collaboratively.

In chemoconvulsant-induced epilepsy models, microglia are activated and produce pro-inflammatory mediators immediately following seizure onset (8). Activated microglia can decrease the seizure threshold in animal models by releasing pro-inflammatory molecules with neuromodulatory properties (9).

Notably, the extent of microglial activation correlates with the seizure frequency in human drug-resistant epilepsy (10). Alternatively, such microglial activation may not persist chronically. For example, pro-inflammatory molecules are detectable in microglia following a seizure but the expression diminishes after several hours (11). Furthermore, although the activation of microglia is well characterized, it is unclear whether these activated microglia affect developing epileptogenic processes directly or through the modulation of other cells, such as subsequent astrocytic activation.

Reactive astrogliosis is also one of the most common pathological features in epilepsy and other brain insults (12,13). Although reactive astrogliosis is considered the consequence of repetitive seizures, some evidence that reactive astrocytes may be responsible for repetitive seizures is available. In the epileptic brain, reactive astrocytes exhibit physiological and molecular changes, such as reduced inward rectifying K^+ current (14), changes in transporters (15), release of gliotransmitters (16), or uncoupling of gap junction (17), that may underlie neuronal hyperexcitability (18). Although astrocytes do not exhibit prominent electrical excitability as observed in neurons, they are able to dynamically regulate calcium using internal stores (19,20). Calcium transients in

astrocytes are thought to modulate the release of a number of gliotransmitters that could influence synaptic function, synapse formation (21–24), and neural circuit excitability (25-27). In particular, several previous studies showed that astrocyte calcium activity could contribute to excitotoxic neuronal death through glutamate release following SE (28,29). However, the functional changes including Ca^{2+} signaling of reactive astrocytes after SE and their causal roles in epileptogenesis remain largely uncertain.

To evaluate the role of inter-glial communication between different types of glial cells in the process of epileptogenesis, we assessed the spatiotemporal dynamics of glial activation following SE. Using cell-type specific manipulation, we show that relative alterations of both, microglia and astrocytes, play causal roles in epileptogenesis. Moreover, reactive glia are temporally distinct and collaboratively contribute to epileptogenesis. Reactive microglia appear first and induce reactive astrocytes in the hippocampus after SE. These reactive astrocytes present larger IP_3R2-mediated Ca^{2+} signals, which are essential for induction of the increased seizure susceptibility after SE. We clearly demonstrate that inhibition of microglial activation reduces astrogliosis, aberrant astrocytic Ca^{2+} signaling, and seizure susceptibility. We therefore conclude that

106 the sequential activation of glial cells; i.e., the initial activation of microglia
107 followed by astrocytic activation, is a cause of epileptogenesis after SE.
108
109 **Results**
110 **Astrocytic activation follows microglial activation after SE**
111 To determine the contributions of glial cells to epileptogenesis, we used the
112 pilocarpine model of epilepsy in mice, a model known to be highly isomorphic
113 with human temporal lobe epilepsy (30,31). Repeated low doses of pilocarpine
114 (100 mg kg^{-1}) were injected intraperitoneally (i.p.) until the onset of SE (Fig 1A).
115 This ramping protocol has been shown to reduce mortality after SE (32,33). To
116 investigate how glial cell activation affects the epileptogenic process, we first
117 examined the spatiotemporal pattern of microglial and astrocytic activation in
118 the hippocampus following SE. We initially assessed microglial and astrocytic
119 activation with immunohistochemistry using cell-type-specific activation markers
120 at 1, 3, 7, and 28 days after SE (Fig 1B and 1D). The area of Iba1-positive
121 microglia was significantly increased in CA1 from 1 to 7 days after SE, which
122 was followed by an increase in the area of GFAP-positive astrocytes in CA1
123 from 3 to 28 days after SE (Fig 1C and 1E).

Out of the twenty-nine animals treated with pilocarpine, ten survived the treatment and received a second treatment, 4 weeks after the first SE, to examine whether the first SE increased seizure susceptibility (the lethality in the first SE was 55.2%). A lower dose of pilocarpine was required for the induction of the second SE in mice with prior exposure to pilocarpine-induced SE at 8 weeks of age (PP) compared to those without such exposure (SP) (Fig 1F). In addition, a lower dose of pilocarpine was required for the induction of the second SE compared to the first SE (Fig 1G) To measure the ictal and the interictal epileptiform activity, we performed EEG recordings of the left CA1 area of the dorsal hippocampus. Interictal spikes significantly increased 7 and 28 days after SE (S1 Fig A, B, C, and F). These data indicated that the first SE increased seizure susceptibility even 4 weeks after the first SE. A comparison with the results in Fig 1 suggested that the temporal pattern of astrocyte activation, rather than that of microglia, correlates well with the increase of seizure susceptibility.

Ca^{2+} hyperactivity via IP_3R2 in reactive astrocytes after SE

To examine the SE-induced functional changes in astrocytes, Ca^{2+} imaging was

performed from hippocampal slices prepared from wild-type (WT) and Glast-CreERT2::flx-GCaMP3 mice (34,35). Astrocytes displayed significantly larger Ca^{2+} signals approximately 4 weeks after SE in somata (Fig 2J, 2K, and 2L) (S1 Movie). To test whether hyperactivity of astrocytes is influenced by neuronal hyperactivity, we blocked neuronal transmission by topically applying the voltage-gated sodium channel blocker tetrodotoxin (TTX; 1 μM). TTX did not affect the amplitude of astrocytic Ca^{2+} signals (Fig 2A, 2D, and 2E) (S2 Movie).

To elucidate the molecular mechanisms involved in astrocytic Ca^{2+} hyperactivity, we applied cyclopiazonic acid (CPA; 20 μM) to deplete intracellular calcium stores. CPA significantly reduced the amplitude of astrocytic Ca^{2+} signals after SE (Fig 2B, 2F, and G) (S2 Movie). Then, we applied the membrane-permeable IP_3 receptor antagonist 2-aminoethoxydiphenyl borate (2-APB; 100 μM). 2-APB also significantly reduced the amplitude of astrocytic Ca^{2+} signals after SE (Fig 2C, 2H, and 2I) (S4 Movie). To confirm that astrocytic Ca^{2+} hyperactivity is completely dependent on the IP_3 receptor, we performed Ca^{2+} imaging in IP_3R2 knockout (KO) mice (36). The amplitude of astrocytic Ca^{2+} signals after SE was significantly decreased in IP_3R2KO mice compared with that in WT (Fig 2J, 2K, 2L, 2M, and 2N). The

frequency of astrocytic Ca^{2+} signals after SE was also significantly decreased in IP_3R2KO mice (Fig 2M and 2N) (S1 Movie). These results suggested that astrocytic Ca^{2+} hyperactivity after SE should be dependent on IP_3R2-mediated Ca^{2+} release from internal stores.

IP_3R2KO mice exhibit rescue of the increased seizure susceptibility

To clarify the role of astrocytic Ca^{2+} hyperactivity after SE in epileptogenesis, we investigated seizure susceptibility after SE in IP_3R2KO mice (36). No differences in the dose of pilocarpine required for the induction of the first SE were observed between IP_3R2KO and WT mice (Fig 1F and 2O). These data indicated that IP_3R2-mediated Ca^{2+} signaling in astrocytes does not alter the acute responses to pilocarpine.

In IP_3R2KO mice, the area of Iba1-positive microglia was significantly increased in CA1 at 1 day after SE, suggesting that microglial activation after SE was comparable in IP_3R2KO and WT mice (S2 Fig). However, there was no significant change in the dose of pilocarpine required for the induction of the second SE in SP compared with PP mice (Fig 2O). Sixteen animals were treated with pilocarpine, out of which ten survived, and received the second

178 treatment, (the lethality in the first SE was 37.5%.) There was no significant
179 change in the dose of pilocarpine required for the induction of the first and
180 second SE in IP_3R2KO mice (Fig 2P). In controlled conditions, there was no
181 significant change in the number of interictal spikes in IP_3R2KO mice when
182 compared with WT mice (S1 Fig F). In addition, interictal spikes were
183 significantly reduced 28 days after SE in IP_3R2KO mice, compared with WT
184 mice (S1 Fig E and F). These results suggested that IP_3R2-mediated astrocytic
185 Ca^{2+} hyperactivity is essential for the induction of the increased seizure
186 susceptibility after SE.
187
188 **Microglia inhibition reduces activated astrocyte morphology**
189 Our data indicated temporal differences between activation of microglia and
190 astrocytes; i.e., earlier and later onset after SE, respectively. To reveal features
191 of the activated microglia after SE, we investigated the changes in mRNA levels
192 of pro-inflammatory cytokines that are relevant to microglial activation by
193 quantitative reverse transcription-polymerase chain reaction (RT-PCR) (Fig 3A,
194 3B, and 3C). SE increased *Tnf* and *Il1b* mRNA in the hippocampus at 1 day
195 after SE (Fig 3B and 3C). To explore the microglia-triggered astrocyte

196 activation, we investigated microglial functional changes after SE. Among
197 several molecules tested, we found that *Tnf* and *Il1b* mRNAs were also
198 significantly upregulated in the isolated hippocampal microglia at 1 day after SE
199 (Fig 3A).

200 To clarify whether microglial activation is required for astrogliosis, we
201 investigated the effect of post-treatment with the inhibitor, minocycline (Fig 3D)
202 (37–39). To confirm the efficacy of minocycline in this protocol, microglial
203 activation was assessed by immunohistochemistry and quantitative RT-PCR.
204 Minocycline post-treatment prevented the increase in the area of Iba1-positive
205 cells in CA1 at 3 days after the first SE (Fig 3E and 3G) along with an increase
206 in *Tnf* but not *Il1b* mRNA in the hippocampus at 1 day after the first SE (Fig 3I
207 and 3J). Notably, microglia inhibition with minocycline post-treatment prevented
208 the increase in the area of GFAP-positive cells in CA1 at 28 days after the first
209 SE (Fig 3F and 3H).

210 To further confirm that acute microglial activation plays an important role in
211 the morphological activation of astrocytes after SE, we applied PLX5622, a
212 CSF1R antagonist, to deplete microglia (Fig 3K) (40–42). PLX5622 treatment
213 prevented the increase in the area of Iba1-positive cells in CA1 from 1 to 7 days

after the first SE (Fig 3L and 3N). In addition, *Aif1* and *Tnf* mRNA levels were significantly decreased at 1 day after SE with PLX5622 treatment compared with those in the control diet group (Fig 3P). Similarly, the increased area of GFAP-positive astrocytes in CA1 from 7 to 28 days after SE in control diet (AIN-76A) mice was prevented in PLX5622 treated mice (Fig 3M and 3O). To identify the optimal timing of microglial inhibition to prevent astrogliosis, we applied PLX5622 from 3 weeks after SE (Fig 4A). This later PLX5622 treatment decreased the area of Iba1-positive cells in CA1 at 28 days after the first SE (Fig 4B and 4D) but did not prevent the increased area of GFAP-positive astrocytes (Fig 4C and 4E). These findings showed that the initial reactive microglia are required to induce morphological activation of astrocytes after SE.

Microglia inhibition reduces astrocytic Ca^{2+} hyperactivity

We then investigated whether microglial activation is required for astrocytic Ca^{2+} hyperactivity after SE. We also used a pharmacological approach to inhibit the early microglial activation after SE. Microglia inhibition with minocycline reduced the larger and frequent Ca^{2+} signals of astrocytes (S5 Movie) (Fig 5A, 5B, 5C, 5D, and 5E). Similarly, the amplitude and frequency of fluo-4AM-labeled

astrocytic Ca^{2+} signaling after SE were significantly increased in control diet (AIN-76A) mice (Fig 5F, 5H, 5I, 5J, and 5K) (S6 Movie). Conversely, the larger and frequent Ca^{2+} signals after SE were significantly reduced by the PLX5622 treatment (Fig 5G, 5L, 5M, 5N, and 5O) (S7 Movie). These results indicated that acute microglial activation is essential for the changes of astrocytic Ca^{2+} activity after SE.

Microglia inhibition rescues enhanced seizure susceptibility

Finally, we tested whether microglia inhibition rescued the increased seizure susceptibility following SE. Eighteen animals were treated with pilocarpine and minocycline, ten mice survived the treatment, and received a second treatment (the lethality in the first SE was 44.4%). Post-treatment with minocycline following the first SE prevented the increased seizure susceptibility (Fig 6A and 6B). No difference was observed between control diet and PLX5622-treated mice in the dose of pilocarpine required for the induction of the first SE (Fig 6C). Furthermore, there was no significant change in the number of interictal spikes in PLX5622-treated mice when compared with WT mice (S1 Fig F). These results indicated that microglia inhibition does not alter the acute responses to

pilocarpine. In contrast, a lower dose of pilocarpine was required for the induction of the second SE in control mice compared with that in PLX5622-treated mice (Fig 6D). Consistent with this, unlike the enhanced seizure susceptibility observed in control mice following the first SE (as indicated by the reduced dose of pilocarpine required to induce the second vs. the first SE), there was no significant change in the dose of pilocarpine required for the induction of the first or second SE in PLX5622-treated mice (Fig 6E and 6F) Fifteen animals were treated with pilocarpine and control diet, and the ten surviving mice received a second treatment (the lethality in the first SE was 33.3%.) Twenty animals were treated with pilocarpine and PLX5622, and ten survived, and received a second treatment (the lethality in the first SE was 60.0%). In addition, interictal spikes were significantly reduced 7 and 28 days after SE in PLX5622-treated mice, compared with WT mice (S1 Fig D and F). In contrast, a lower dose of pilocarpine was required for the induction of the second SE in later PLX5622 treatment mice, similar to that in control diet mice (Fig 6G, 6H, 6I, and 6J). Twenty-four animals were treated with pilocarpine and control diet, and the ten surviving mice received a second treatment. The lethality in the first SE was 58.3%. Seventeen animals were treated with

pilocarpine and PLX5622 later phase, and ten survived, receiving a second treatment. The lethality in the first SE was 41.2%. These data suggested that the inhibition of initial microglial activation rescues the increased seizure susceptibility.

Discussion

Here, we demonstrate that SE induces sequential activation of glial cells; i.e., the initial activation of microglia, followed by astrocytic activation, which is essential for seizure susceptibility or epileptogenesis. The main findings in the present study are as follows: 1. Microglia are activated and pro-inflammatory cytokines of microglia are increased immediately after SE; 2. Reactive astrocytes, which exhibit larger IP_3R2-mediated Ca^{2+} signals, appear following microglial activation after SE; 3. Genetic deletion of IP_3R2 rescues both the aberrant Ca^{2+} signals in astrocytes and the increased seizure susceptibility; 4. Pharmacological inhibition of microglial activation or deletion of microglia at early phase after SE reduces astrogliosis along with aberrant Ca^{2+} signals of astrocytes, and rescues the increased seizure susceptibility. These findings indicate that initially activated microglia are responsible for the subsequent

induction of epileptogenic reactive astrocytes in vivo. The limitation of this study is that the severity of epilepsy was not evaluated by spontaneous recurrent seizures, but was evaluated by changes in the threshold of pilocarpine-induced seizures and interictal spikes. However, overall our findings suggest that the therapeutic target to prevent epilepsy after status epilepticus should be shifted from microglia (early phase) to astrocytes (late phase).

Microglial and astrocytic activation is a common feature of various central nervous system (CNS) disorders including epilepsy (43–46). However, the pathological significance and spatiotemporal pattern of microglial and astrocytic activation in the epileptogenic process have not been carefully addressed. Microglial response to SE occurs immediately, with reactive microglia playing both detrimental and beneficial roles during acute seizures (47). Although activated microglia exhibit a neuroprotective role via the P2Y12 receptor in the acute phase, they exert proconvulsive effects through the production of pro-inflammatory cytokines such as IL-1β (11), TNF (48), and IL-6 (49,50). However, such increase of purinergic receptors and pro-inflammatory cytokines after SE may be transient (11), and it is unknown how this transient microglial activation including pro-inflammatory cytokines causes long-term epileptic potential. Here,

we found that inhibiting microglia at the acute phase (0 to 7 days after SE) but not the late phase (21 to 28 days after SE) reduced susceptibility to the second SE, suggesting that activated microglia trigger the epileptogenic process including astrocytic activation, but do not exert a direct proconvulsive effect on the later phase after SE.

In the present study, we demonstrate that astrocytic activation develops slowly starting 7 days after SE, is long lasting, and still observed when mice show increased seizure susceptibility. Astrogliosis is thought to contribute to the pathophysiology of epilepsy (51–53). Some previous reports show dysregulation of astrocyte functions, such as K^+ ion homeostasis (14), neurotransmitter buffering (15), gliotransmission (16), or purinergic signaling (54, 55), can actively contribute to hyperexcitation of neuronal networks and progression of seizures. However, the role of astrogliosis in epileptogenesis is largely unknown. In particular, it is important to determine whether activated astrocytes play a proconvulsive or anticonvulsive role in the epileptic brain. It has been proposed that astrocytic Ca^{2+} signaling contributes to the induction of epileptic seizures and neuronal cell loss by seizures (24,31,32,56). In this study, we observed larger Ca^{2+} signals in the somatic regions of astrocytes in the latent

phase of epileptogenesis. Analysis of the Ca^{2+} signals in astrocytes suggests that these Ca^{2+} signals are mediated by IP_3R2. Notably, we found that genetic deletion of IP_3R2 is sufficient to rescue the increased seizure susceptibility and reduce astrogliosis. Our study thus suggests that IP_3R2-mediated Ca^{2+} signaling in reactive astrocytes plays a proconvulsive role in the epileptic brain and can contribute to epileptogenesis.

Astrocytic Ca^{2+} signals may contribute to epileptogenesis through several mechanisms. Astrocytes impact neural circuit excitability directly by releasing “gliotransmitters”, such as glutamate (25,57,58). Astrocytes also increase neuronal excitability by forming new circuits through the release of synaptogenic molecules (23,59). However, the functional consequences of these changes in the context of epileptogenesis remain to be determined. As Ca^{2+} ions serve as a ubiquitous intracellular signal in the regulation of numerous cellular processes, including exocytosis, proliferation, and gene expression, it is also likely to regulate many processes in the induction or maintenance of reactive astrocytes (60,61). Since it has been reported that the Ca^{2+} signals in astrocytes could contribute to ictogenesis (27,29), we cannot disregard the possibility that IP_3R2 may contribute to neural excitability and microglial activation after SE. We

340 demonstrate that SE induces neither an increase in Ca^{2+} excitation in astrocytes
341 nor proconvulsive effects in IP_3R2KO mice, suggesting that enhanced Ca^{2+}
342 signals in astrocytes are likely responsible for epileptogenesis.
343 In animal models of epilepsy, reactive astrocytes undergo extensive
344 physiological changes involving not only Ca^{2+} signaling but also ion and
345 neurotransmitter homeostasis along with intracellular and extracellular water
346 content, which can cause neuronal hyperexcitability (17,62–64). The relative
347 importance of such functional changes of astrocytes to epileptogenesis will be
348 investigated in future studies. Recently, it has been reported that activated
349 microglia can induce neurotoxic reactive astrocytes (i.e., A1 astrocytes), which
350 release unidentified neurotoxic factors (41,65). Thus, whether astrogliosis after
351 SE results in a similar phenotype to A1 astrocytes and whether IP_3-mediated
352 Ca^{2+} signals contribute to the induction of neurotoxic phenotype (61) represent
353 relevant issues to be addressed in future investigations. However, it was also
354 reported that these functional changes of astrocytes, including gap junction
355 dysfunction (17), could occur before the increase is observed in GFAP
356 immunostaining, astrocytic Ca^{2+} signals, or Iba1 immunostaining, investigated in
357 this study. Although whether the astrocytes induced by activated microglia are

in a primarily neurotoxic or neuroprotective state remains largely unknown, our data suggest that the reactive astrocytes induced by activated microglia after SE exert proconvulsive effects in the epileptic brain.

In this study, we also demonstrate that pro-inflammatory cytokines of microglia are increased prior to astrocytic activation, suggesting the importance of microglial activation as an initial process of epileptogenesis. Pharmacological inhibition and depletion of microglia significantly blocked the activation of astrocytes and decreased the seizure threshold after SE. Our findings identify that activated microglia likely promote epileptogenesis by inducing the proconvulsive phenotype of astrocytes. Although it has been recognized that microglial activation occurs before reactive astrogliosis in various CNS diseases (66-68), little was known prior to the present study regarding how microglial-astrocytic interactions contribute to the pathophysiology of epilepsy. For example, several previous studies using chemoconvulsant-induced epilepsy models have shown that activated microglia were present immediately after SE and that functional changes occurred, such as upregulation of pro-inflammatory cytokines (8,69,70), purinergic receptors (43), and phagocytosis (44).

Previous reports also revealed that microglia modulate astrocyte activation

via various molecules, especially pro-inflammatory cytokines (71,72). Consistent with this, we found that TNF and IL-1β are significantly upregulated in hippocampal microglia at 1 day after SE. Conversely, microglia inhibition by minocycline prevents the increased mRNA of TNF in the hippocampus at 1 day after the first SE along with subsequent reactive astrogliosis, suggesting a potential role of pro-inflammatory cytokines from microglia in reactive astrogliosis after SE. As the effect of minocycline may not be restricted to microglia, we depleted microglia using a CSF-1 receptor antagonist and found similar results, suggesting that microglial activation occurs through cytokine release. CSF1 receptor antagonist may affect not only microglia, but also peripheral macrophages (73,74), which could contribute to pathophysiology of epilepsy (75-77). Thus, despite the potential problem of specificity owing to the use of pharmacological inhibition of microglia, we clearly show that initial activation of microglia and microglia-derived proinflammatory cytokines likely underlie the subsequent astrogliosis-mediated epileptogenesis. Nevertheless, because the molecular mechanisms underlying the activation of astrocytes triggered by activated microglia have not been fully clarified, other chemical mediators such as ATP may also contribute to activate microglia-mediated

astrogliosis (78). Further investigations using more specific interventions are required to elucidate the precise molecular mechanisms underlying the interaction between microglia and astrocytes.

In summary, our findings identify a sequence of glial activation in the hippocampus that contributes to the epileptogenic process. In this process, microglial activation is identified as a crucial event to induce reactive astrocytes. In turn, astrocytic Ca^{2+} activation, mediated by IP_3R2, plays an important role in the induction of epileptogenesis. Our findings add to the emerging view that reactive astrocytes triggered by microglia have a central role in the pathogenesis of epilepsy and, given the limited progress of neuron-centered epilepsy research over the past several years, suggest reactive glial cells as promising new targets for the development of alternative and more specific antiepileptic drugs.

Methods

Animals

All studies used male C57BL/6J mice (SLC Japan, Shizuoka, Japan). IP_3R2KO mice on a C57BL/6 background were available from a previous study (36); their generation and maintenance have been previously described in detail. Glast-CreERT2::flx-GCaMP3 mice on a C57BL/6 background were also available from a previous study (34,35); their generation and maintenance have been previously described in detail. In the present study, we performed immunohistochemistry and confirmed that GCaMP3 was co-localized with GFAP, an astrocyte marker, but not with Iba1 or NeuN (S3 Fig and S1 Table). Overall, Ca^{2+} signals detected by GCaMP3 were mainly detected from astrocytes.

Mice were housed on a 12 h light (6 am)/dark (6 pm) cycle with ad libitum access to water and rodent chow. The animals were allowed to adapt to laboratory conditions for at least 1 week before starting the experiments.

Animal treatments

The first SE was induced in 8-week-old male mice by the administration of pilocarpine and the second SE was induced 4 weeks after the first SE. A low dose

425 of 100 mg kg^{-1} pilocarpine (Wako, 161-07201) per injection was administered i.p.
426 every 20 min until the onset of Racine scale stage 5 seizures. Scoporamin methyl
427 bromide (1 mg kg^{-1}, i.p., Wako, 198-07971) was administered 30 min prior to
428 pilocarpine injection to reduce its peripheral effects (32,33). Seizures were
429 terminated with pentobarbital (20 mg kg^{-1}, i.p., Kyoritu Seiyaku) when mice
430 experienced stage 5 seizures for 30 min. Behavior of pilocarpine-treated mice
431 was observed for 1 h after SE. To examine whether the first SE increased seizure
432 susceptibility, the second SE was induced 4 weeks after the first SE using the
433 same protocol.

434 To establish whether minocycline inhibits acute seizure-induced microglial
435 activation, mice were administered i.p. with saline or minocycline (25 mg kg^{-1}) 1
436 h after pilocarpine-SE induction and for the following two consecutive days (37–
437 39). Microglia were also depleted from mice by treatment with the CSF1R
438 antagonist, PLX5622 (Plexxikon), formulated in AIN-76A rodent chow (Research
439 Diets). Mice were treated with PLX5622 (1200 mg kg^{-1} Chow) or a matched
440 control diet (AIN-76A) for seven days before SE and for the following seven
441 consecutive days (40–42).

442

EEG acquisition

The mice were deeply anesthetized with isoflurane. For EEG recordings, a bipolar electrode was implanted at the left CA1 area of the dorsal hippocampus (AP = -1.8 mm, ML = +1.6 mm, DV = -2.0 mm). The electrode was fixed to the skull with dental cement. Animals were allowed to recover for 5 to 7 days before EEG recording. EEGs were recorded in freely moving mice using a digital acquisition system (PowerLab 26T, ADInstruments), for at least 2 hour per day. EEG data were collected at a sampling rate of 2000 Hz. Data were acquired, digitized, and analyzed off-line using Labchart 8 software (ADInstruments). The artifacts in the raw EEG traces were manually identified and excluded from the analyses of interictal spikes.

Immunohistochemistry

The mice were deeply anesthetized with pentobarbital and perfused transcardially with phosphate buffered saline (PBS), followed by 4% (w/v) paraformaldehyde in PBS. The brains were removed, postfixed overnight, then cryoprotected with 30% (w/v) sucrose in PBS for two days. The brains were frozen and coronal sections (20 μm) were cut using a cryostat (Leica CM1100).

Slices were washed with PBS three times and treated with 0.1% Triton-X100/10% NGS for 1 h to block nonspecific binding. The sections were incubated for two days at 4 °C with the following primary antibodies: monoclonal rat anti-GFAP (1:2000; Thermo Fisher Scientific, 13-0300), monoclonal mouse anti-NeuN (1:500; Millipore, MAB377), polyclonal rabbit anti-Iba1 (1:1000; Wako, 019-19741), polyclonal chicken anti-GFP antibody (1:1000, Thermo Fisher Scientific, A10262), and monoclonal rabbit anti-NeuN (1:1,000; Millipore, MABN140). The sections were washed three times with PBS and then incubated for 2 h at room temperature with secondary antibodies: Alexa 488- or Alexa 546-conjugated polyclonal goat anti-mouse/rat/rabbit or chicken IgGs (1:500; Invitrogen, A11029/Thermo Fisher Scientific, A-11081/Invitrogen, A11035/Thermo Fisher Scientific, A11039). After washing slices with PBS three times, they were mounted with Vectashield Mounting Medium (Vector Laboratories). Fluorescence images were obtained using a confocal laser microscope system (FV-1000; Olympus) or Keyence fluorescence microscope (BZX-700).

Standard quantitative RT-PCR

Total RNA was isolated and purified from tissues using the RNeasy Lipid Tissue

Mini Kit (Qiagen) according to the manufacturer's instructions. RT-PCR amplifications were performed using the One Step PrimeScript RT-PCR Kit (TaKaRa Bio). RT-PCR amplifications and real-time detection were performed using an Applied Biosystems 7500 Real-Time PCR System. The thermocycling parameters were as follows: 5 min at 42 °C for reverse transcription, 10 s at 95 °C for inactivation of the RT enzyme, and 40 cycles of denaturation (5 s at 95 °C) and annealing or extension (34 s at 60 °C). Relative gene expression was calculated using *Gapdh* expression as a housekeeping gene. All primer probe sets and reagents were purchased from Applied Biosystems: rodent *Gapdh* (4308313), mouse *Tnf* (Mm00443260_g1), mouse *Il1b* (Mm00434228_m1).

Dissociated cell suspensions from adult mouse brain

Three 8-week old male mice were perfused with PBS after anesthesia to eliminate serum vesicles and hippocampi were dissected to comprise one sample. Tissue dissociation was performed using the gentleMACS dissociator and the Adult Brain Dissociation Kit (Miltenyi Biotec) according to the manufacturer's protocol. Briefly, brain tissue was minced and digested with a proprietary enzyme solution on the gentleMACS dissociator adult brain program. The cells were then

incubated with anti-mouse CD11b-coated microbeads (Miltenyi Biotec) for 10 min at 4 °C. The cell-bead mix was then washed to remove unbound beads. Prior to antibody labeling, nonspecific binding to the Fc receptor was blocked using the FcR Blocking Reagent (Miltenyi Biotec). Cells were suspended in PBS with 0.5% bovine serum albumin and the cell suspension was loaded onto an LS Column (Miltenyi Biotec), which was placed in the magnetic field of a QuadroMACS™ Separator (Miltenyi Biotec). The magnetically labeled CD11b positive cells were retained within the column and eluted as the positively selected cell fraction after removing the column from the magnet.

Microfluidic quantitative RT-PCR

Total RNA was extracted from dissociated cells using the RNeasy Lipid Tissue Mini Kit (Qiagen) and cDNA synthesis performed using the PrimeScript RT-PCR Kit (Perfect Real Time) (TaKaRa Bio). For pre-amplification, up to 100 qPCR assays (primer or probe sets in 20x stock concentration) were pooled and diluted to a 0.2x concentration. For microfluidic qPCR, 1.25 µL of each cDNA sample was pre-amplified using 1 µL of TaqMan pre-amplification master mix (PN 100-5580, Fluidigm), 1.25 µL of the primer pool, and 1.5 µL of water. Pre-amplification

was performed using a 2 min 95 °C denaturation step and 14 cycles of 15 s at 95 °C and 4 min at 60 °C. Microfluidic quantitative RT-PCR reactions were performed using the 96x96 chips and included 2–3 technical replicates for each combination of sample and assay. For sample mixtures, 2.7 µL pre-amplification product was combined with 0.3 µL of 20x GE Sample Loading Reagent (85000746, Fluidigm) and 3 µL of 2x PCR master mix (4324020, Thermo Fisher Scientific), of which 5 µL of was loaded into sample wells. For assay mixtures, equal volumes of TaqMan assay and 2x Assay Loading Reagent (PN85000736, Fluidigm) were combined, and 5 µL of the resulting mixture was loaded into multiple assay wells. RT-PCR amplifications and real-time detection were performed using the BioMarkHD Real-Time PCR System (Fluidigm). Data from Fluidigm runs were manually checked for reaction quality prior to analysis, and Ct values for each gene target were normalized to Ct values for housekeeping genes. All primer probe sets and reagents were purchased from Integrated DNA Technologies: rodent *Gapdh* (Mm.PT.39a.1), mouse *Tnf* (Mm.PT.58.12575861), mouse *Il1b* (Mm.PT.58.41616450), mouse *Cx3cr1* (Mm.PT.58.17555544), mouse *CD45* (Mm.PT.58.7583849), mouse *CD11b* (Mm.PT.58.14195622), mouse *CD68* (Mm.PT.58.32698807), mouse *CD206* (Mm.PT.58.42560062), mouse *Il6*

(Mm.PT.58.10005566), mouse *Ifng* (Mm.PT.58.41769240), mouse *Il4* (Mm.PT.58.32703659), mouse *Il10* (Mm.PT.58.13531087), and mouse *Tgfb* (Mm.PT.58.11254750).

Preparation of brain slices and Ca^{2+} imaging

The methods used have been described previously (61,79). Briefly, 8-week-old male mice were anesthetized with pentobarbital (100 mg kg^{-1}, i.p.). Cold cutting ACSF, composed of 92 mM NaCl, 2.5 mM KCl, 1.2 mM NaH_2PO_4, 30 mM $NaHCO_3$, 20 mM HEPES, 25 mM D-glucose, 5 mM sodium ascorbate, 2 mM thiourea, 3 mM sodium pyruvate, 10 mM $MgCl_2$, and 0.5 mM $CaCl_2$ saturated with 95% O_2–5% CO_2, was perfused transcardially. Coronal slices of the hippocampus (300 µm) were cut using a vibrating microtome (Pro7, Dosaka) in cutting ACSF. Slices were incubated at 34 °C for 10 min in recovery ACSF, composed of 93 mM N-methyl-D-glucamine, 93 mM HCl, 2.5 mM KCl, 1.2 mM NaH_2PO_4, 30 mM $NaHCO_3$, 20 mM HEPES, 25 mM D-glucose, 5 mM sodium ascorbate, 2 mM thiourea, 3 mM sodium pyruvate, 10 mM $MgCl_2$, and 0.5 mM $CaCl_2$ saturated with 95% O_2–5% CO_2, and subsequently stored in ACSF comprising 124 mM NaCl, 2.5 mM KCl, 1.2 mM NaH_2PO_4, 24 mM $NaHCO_3$, 5 mM HEPES, 12.5 mM D-

glucose, 5 mM sodium ascorbate, 2 mM thiourea, 3 mM sodium pyruvate, 2 mM $MgCl_2$, and 2 mM $CaCl_2$ saturated with 95% O_2 and 5% CO_2 at room temperature. After 1 h of recovery, slices were submerged in ACSF at approximately 32 °C. Slices were imaged using an Olympus Fluoview FV1000MPE two-photon laser scanning microscope equipped with a Maitai HP DS-OL laser (Spectra-Physics). We used a 920 nm laser and 495-540 nm bandpass emission filter. Astrocytes were selected from the CA1 stratum radiatum region and were typically 30–50 μm from the slice surface. Images were gathered using a 40× water immersion lens with a numerical aperture of 0.80.

For Fluo-4AM measurements, we dropped 2.5 μL Fluo-4AM (2 mM) onto the hippocampal slices followed by incubation in ACSF for 60 min, then transferred the slices to dye-free ACSF for at least 30 min prior to experimentation. The final concentration of Fluo4-AM was 5 μM with 0.02% Pluronic F–127. Astrocytes were selected from the CA1 stratum radiatum region and were typically 30–50 μm from the slice surface. TTX (1 μM), 2-APB (100 μM), and CPA (20 μM) were solubilized in ACSF. Baseline astrocytic activity was recorded prior to drug application. Subsequently, drugs were applied onto the slice for 10 min and astrocytic activity was recorded for 10 min.

Image analysis

Images were acquired using inverted confocal laser-scanning systems (Olympus FV-1000) at 40× magnification with a 1.30 numerical aperture objective lens. Information regarding z-stack images is described in the figure legends. Astrocytes were selected from the CA1 stratum radiatum region and imaged based on GFAP immunostaining. Microglia were imaged based on Iba1 immunostaining at the CA1 stratum radiatum region. Subsequent images were processed and quantified using ImageJ (US National Institutes of Health; NIH). For the quantitative analysis of the area containing Iba1 positive microglia, we randomly chose three fields per mouse. Images were converted to gray scale and the quantification threshold was set constantly for all specimens within each experimental group. The percentage of Iba1-positive area was calculated by dividing the area of Iba1-positive region by the total area of the region of interest. For the quantitative analysis of the area containing GFAP positive astrocyte, the percentage of GFAP-positive area was calculated using the same method used to quantify Iba1-positive microglia.

The methods used for Ca^{2+} imaging data analysis have been described

previously (56,70). Briefly, imaging data were analyzed using ImageJ. We selected regions of interest from somatic regions of astrocytes by visual examination of the time lapse image. Using these regions of interest, raw fluorescence intensity values (F) were taken from the original videos and converted to delta F/F (dF/F) in Originlab (Origin Lab Corp.). We analyzed Ca^{2+} signals when their dF/F values were greater than 0.2. We analyzed Ca^{2+} signals and their amplitude (dF/F) and duration (full width at half maximum) using the Originlab “peak analysis” function.

Statistical analysis

All statistical analyses were performed using SPSS version 19.0 (SPSS Inc.) software. Data are presented as the mean ± SEM. Most data were analyzed using one-way ANOVA followed by Dunnett’s multiple post hoc test for comparing more than three samples, and two-sample unpaired *t*-tests. *P* values <0.05 were considered as statistically significant.

Study approval

All experimental procedures were performed in accordance with the “Guiding

Principles in the Care and Use of Animals in the Field of Physiologic Sciences" published by the Physiologic Society of Japan and with the previous approval of the Animal Care Committee of Yamanashi University (Chuo, Yamanashi, Japan).

Author contributions

F.S. and S.K. conceived and designed the research. F.S. performed most of the experiments, analyzed the data, and wrote the manuscript. H.T. contributed to the immunohistochemistry experiments. K.S. contributed to the MACS experiments. Y.S., E.S., and S.K. analyzed the data. K.M. provided IP3R2KO mice. H.H., D.C., and J.N. contributed to the EEG experiments. K.S., M.A., and S.K. supervised the project. All of the authors discussed and commented on the manuscript.

Acknowledgements

This work was supported by JSPS KAKENHI Grant Numbers JP16H04669, JP16K19634, JP18K15701, JP18H05121, JP19H04746, 20H05902, 20H05060, Scientific Research on Innovative Areas 25117003, CREST JPMJCR14G2, AMED-CREST (25gm1310008), the Mitsubishi Science Foundation, the Takeda Science Foundation, Intramural Research Grant (28-4) for Neurological and

623 Psychiatric Disorders of NCNP, and a Grant for the Cutting Edge Brain
624 Sciences from the University of Yamanashi. We thank Dr. K. Takanashi, Mr. R.
625 Komatsu, Mrs. Y. Fukasawa, Mrs. M. Tachibana, Mrs. Y. Koseki, and Mrs. Y.
626 Hoshino (Univ. Yamanashi) for technical assistance, and all members of the
627 Koizumi Laboratory for critical discussion.
628

References

1. Engel J Jr. Mesial temporal lobe epilepsy: what have we learned? *Neuroscientist*. 2001;7(4):340–352.

2. Herman ST. Epilepsy after brain insult: targeting epileptogenesis. *Neurology*. 2002;59(9 Suppl 5):S21–26.

3. French JA, et al. Characteristics of medial temporal lobe epilepsy: I. Results of history and physical examination. *Ann Neurol*. 1993;34(6):774–780.

4. Rakhade SN, Jensen FE. Epileptogenesis in the immature brain: emerging mechanisms. *Nat Rev Neurol*. 2009;5(7):380–391.

5. Binder DK, Steinhauser C. Functional changes in astroglial cells in epilepsy. *Glia*. 2006;54(5):358–368.

6. Seifert G, Steinhauser C. Neuron-astrocyte signaling and epilepsy. *Exp Neurol*. 2013;244:4–10.

7. Shapiro LA, Wang L, Ribak CE. Rapid astrocyte and microglial activation following pilocarpine-induced seizures in rats. *Epilepsia*. 2008;49 Suppl 2:33–41.

8. Benson MJ, Manzanero S, Borges K. Complex alterations in microglial M1/M2 markers during the development of epilepsy in two mouse models. *Epilepsia*. 2015;56(6):895–905.

9. Vezzani A, French J, Bartfai T, Baram TZ. The role of inflammation in epilepsy. *Nat Rev Neurol*. 2011;7(1):31–40.

10. Boer K, et al. Evidence of activated microglia in focal cortical dysplasia. *J Neuroimmunol*. 2006;173(1-2):188–195.

11. Vezzani A, et al. Functional role of inflammatory cytokines and antiinflammatory molecules in seizures and epileptogenesis. *Epilepsia*. 2002;43 Suppl 5:30–35.

12. Cendes F, Sakamoto AC, Spreafico R, Bingaman W, Becker AJ. Epilepsies associated with hippocampal sclerosis. *Acta Neuropathol*. 2014;128(1):21–37.

13. Morizawa YM, et al. Reactive astrocytes function as phagocytes after brain ischemia via ABCA1-mediated pathway. *Nat Commun*. 2017;8(1):1598.

14. Haj-Yasein NN, et al. Evidence that compromised K+ spatial buffering contributes to the epileptogenic effect of mutations in the human Kir4.1 gene (KCNJ10). *Glia*. 2011;59(11):1635–1642.

15. Tanaka K, et al. Epilepsy and exacerbation of brain injury in mice lacking the glutamate transporter GLT-1. *Science*. 1997;276(5319):1699–1702.

16. Bezzi P, et al. Astrocytes contain a vesicular compartment that is competent for regulated exocytosis of glutamate. *Nat Neurosci*. 2004;7(6):613–620.

17. Bedner P, et al. Astrocyte uncoupling as a cause of human temporal lobe epilepsy. *Brain*. 2015;138(Pt 5):1208–1222.

18. Devinsky O, Vezzani A, Najjar S, De Lanerolle NC, Rogawski MA. Glia and epilepsy: excitability and inflammation. *Trends Neurosci*. 2013;36(3):174–184.

19. Charles AC, Merrill JE, Dirksen ER, Sanderson MJ. Intercellular signaling in glial cells: calcium waves and oscillations in response to mechanical stimulation and glutamate. *Neuron*. 1991;6(6):983–992.

20. Cornell-Bell AH, Finkbeiner SM, Cooper MS, Smith SJ. Glutamate induces calcium waves in cultured astrocytes: long-range glial signaling. *Science*. 1990;247(4941):470–473.

21. Allen NJ, Eroglu C. Cell biology of astrocyte-synapse interactions. *Neuron*. 2017;96(3):697–708.

22. Araque A, et al. Gliotransmitters travel in time and space. *Neuron*. 2014;81(4):728–739.

23. Kim SK, et al. Cortical astrocytes rewire somatosensory cortical circuits for peripheral neuropathic pain. *J Clin Invest*. 2016;126(5):1983–1997.

24. Alvarez-Ferradas C, et al. Enhanced astroglial Ca2+ signaling increases excitatory synaptic strength in the epileptic brain. *Glia*. 2015;63(9):1507–1521.

683 25. Halassa MM, Fellin T, Haydon PG. The tripartite synapse: roles for
684 gliotransmission in health and disease. *Trends Mol Medi*. 2007;13(2):54–63.
685 26. Szokol K, et al. Augmentation of Ca (2+) signaling in astrocytic endfeet in the
686 latent phase of temporal lobe epilepsy. *Frontiers in cellular neuroscience*.
687 2015;9:49.
688 27. Heuser K, et al. Ca^{2+} Signals in Astrocytes Facilitate Spread of Epileptiform
689 Activity. *Cerebral cortex*. 2018;28:4036-4048.
690 28. Ding S, et al. Enhanced astrocytic Ca2+ signals contribute to neuronal
691 excitotoxicity after status epilepticus. *J Neurosci*. 2007;27(40):10674–10684.
692 29. Tian GF, et al. An astrocytic basis of epilepsy. *Nat Med*. 2005;11(9):973–981.
693 30. Curia G, Longo D, Biagini G, Jones RS, Avoli M. The pilocarpine model of
694 temporal lobe epilepsy. *J Neurosci Methods*. 2008;172(2):143–157.
695 31. Levesque M, Avoli M, Bernard C. Animal models of temporal lobe epilepsy
696 following systemic chemoconvulsant administration. *J Neurosc Methods*.
697 2016;260:45–52.
698 32. Clasadonte J, Dong J, Hines DJ, Haydon PG. Astrocyte control of synaptic
699 NMDA receptors contributes to the progressive development of temporal lobe
700 epilepsy. *Proc Natl Acad Sci U S A*. 2013;110(43):17540–17545.

701 33. Groticke I, Hoffmann K, Loscher W. Behavioral alterations in a mouse model
702 of temporal lobe epilepsy induced by intrahippocampal injection of kainate.
703 *Experimental neurology*. 2008;213:71-83.
704 34. Mori T, Tanaka K, Buffo A, Wurst W, Kuhn R, Gotz M. Inducible gene deletion
705 in astroglia and radial glia--a valuable tool for functional and lineage analysis. *Glia*.
706 2006;54(1):21–34.
707 35. Zariwala HA, et al. A Cre-dependent GCaMP3 reporter mouse for neuronal
708 imaging in vivo. *J Neurosci*. 2012;32(9):3131–3141.
709 36. Futatsugi A, et al. IP3 receptor types 2 and 3 mediate exocrine secretion
710 underlying energy metabolism. *Science*. 2005;309(5744):2232–2234.
711 37. Abraham J, Fox PD, Condello C, Bartolini A, Koh S. Minocycline attenuates
712 microglia activation and blocks the long-term epileptogenic effects of early-life
713 seizures. *Neurobiol Dis*. 2012;46(2):425–430.
714 38. Hirayama Y, et al. Astrocyte-mediated ischemic tolerance. *J Neurosci*.
715 2015;35(9):3794–3805.
716 39. Matsuda T, et al. TLR9 signalling in microglia attenuates seizure-induced
717 aberrant neurogenesis in the adult hippocampus. *Nat Commun*. 2015;6:6514.
718 40. Dagher NN, et al. Colony-stimulating factor 1 receptor inhibition prevents

719 microglial plaque association and improves cognition in 3xTg-AD mice. *J*
720 *Neuroinflamm*. 2015;12:139.
721 41. Shinozaki Y, et al. Transformation of astrocytes to a neuroprotective
722 phenotype by microglia via P2Y1 receptor downregulation. Cell Rep.
723 2017;19(6):1151-1164.
724 42. Valdearcos M, et al. Microglia dictate the impact of saturated fat consumption
725 on hypothalamic inflammation and neuronal function. *Cell Rep*. 2014;9(6):2124–
726 2138.
727 43. Avignone E, Ulmann L, Levavasseur F, Rassendren F, Audinat E. Status
728 epilepticus induces a particular microglial activation state characterized by
729 enhanced purinergic signaling. *J Neurosci*. 2008;28(37):9133–9144.
730 44. Koizumi S, et al. UDP acting at P2Y6 receptors is a mediator of microglial
731 phagocytosis. *Nature*. 2007;446(7139):1091–1095.
732 45. Pekny M, Nilsson M. Astrocyte activation and reactive gliosis. *Glia*.
733 2005;50(4):427–434.
734 46. Sofroniew MV, Vinters HV. Astrocytes: biology and pathology. *Acta*
735 *Neuropathol*. 2010;119(1):7–35.
736 47. Eyo UB, Murugan M, Wu LJ. Microglia-neuron communication in epilepsy.

737 *Glia*. 2017;65(1):5–18.

738 48. Stellwagen D, Beattie EC, Seo JY, Malenka RC. Differential regulation of
739 AMPA receptor and GABA receptor trafficking by tumor necrosis factor-alpha. *J*
740 *Neurosci*. 2005;25(12):3219–3228.

741 49. Campbell IL, et al. Neurologic disease induced in transgenic mice by cerebral
742 overexpression of interleukin 6. *Proc Natl Acad Sci U S A*. 1993;90(21):10061–
743 10065.

744 50. Samland H, et al. Profound increase in sensitivity to glutamatergic- but not
745 cholinergic agonist-induced seizures in transgenic mice with astrocyte production
746 of IL-6. *J Neurosci Res*. 2003;73(2):176–187.

747 51. Coulter DA, Steinhauser C. Role of astrocytes in epilepsy. *Cold Spring Harb*
748 *Perspect Med*. 2015;5(3):a022434.

749 52. Seifert G, Carmignoto G, Steinhauser C. Astrocyte dysfunction in epilepsy.
750 *Brain Res Rev*. 2010;63(1-2):212–221.

751 53. Steinhauser C, Grunnet M, Carmignoto G. Crucial role of astrocytes in
752 temporal lobe epilepsy. *Neuroscience*. 2016;323:157–169.

753 54. Li T, et al. Adenosine kinase is a target for the prediction and prevention of
754 epileptogenesis in mice. *The Journal of clinical investigation.* 2008;118:571-82.

755 55. Boison D. The adenosine kinase hypothesis of epileptogenesis. *Progress in*
756 *neurobiology*. 2008;84:249-262.
757 56. Gomez-Gonzalo M, et al. An excitatory loop with astrocytes contributes to
758 drive neurons to seizure threshold. *PLoS Biol*. 2010;8(4):e1000352.
759 57. Bazargani N, Attwell D. Astrocyte calcium signaling: the third wave. *Nat*
760 *Neurosci*. 2016;19(2):182–189.
761 58. Haydon PG. GLIA: listening and talking to the synapse. *Nat Rev Neurosci*.
762 2001;2(3):185–193.
763 59. Weissberg I, et al. Albumin induces excitatory synaptogenesis through
764 astrocytic TGF-beta/ALK5 signaling in a model of acquired epilepsy following
765 blood-brain barrier dysfunction. *Neurobiol Dis*. 2015;78:115–125.
766 60. Berridge MJ, Bootman MD, Roderick HL. Calcium signalling: dynamics,
767 homeostasis and remodelling. *Nat Rev Mol Cell Biol*. 2003;4(7):517–529.
768 61. Saito K, et al. Aberrant astrocyte Ca(2+) signals "AxCa signals" exacerbate
769 pathological alterations in an Alexander disease model. *Glia*. 2018;66(5):1053–
770 1067.
771 62. Bordey A, Lyons SA, Hablitz JJ, Sontheimer H. Electrophysiological
772 characteristics of reactive astrocytes in experimental cortical dysplasia. *J*

773 *Neurophysiol*. 2001;85(4):1719–1731.

774 63. Bordey A, Sontheimer H. Properties of human glial cells associated with
775 epileptic seizure foci. *Epilepsy Res*. 1998;32(1-2):286–303.

776 64. Steinhauser C, Seifert G, Bedner P. Astrocyte dysfunction in temporal lobe
777 epilepsy: K+ channels and gap junction coupling. *Glia*. 2012;60(8):1192–1202.

778 65. Liddelow SA, et al. Neurotoxic reactive astrocytes are induced by activated
779 microglia. *Nature*. 2017;541(7638):481–487.

780 66. Dheen ST, Kaur C, Ling EA. Microglial activation and its implications in the
781 brain diseases. *Curr Med Chem*. 2007;14(11):1189–1197.

782 67. Kingwell K. Neurodegenerative disease: Microglia in early disease stages.
783 *Nat Rev Neurol*. 2012;8(9):475.

784 68. Shinozaki Y, et al. Microglia trigger astrocyte-mediated neuroprotection via
785 purinergic gliotransmission. *Sci Rep*. 2014;4:4329.

786 69. Riazi K, et al. Microglial activation and TNFalpha production mediate altered
787 CNS excitability following peripheral inflammation. *Proc Natl Acad Sci U S A*.
788 2008;105(44):17151–17156.

789 70. Vezzani A, et al. Interleukin-1beta immunoreactivity and microglia are
790 enhanced in the rat hippocampus by focal kainate application: functional

791 evidence for enhancement of electrographic seizures. *J Neurosci*.
792 1999;19(12):5054–5065.
793 71. John GR, Lee SC, Brosnan CF. Cytokines: powerful regulators of glial cell
794 activation. *Neuroscientist*. 2003;9(1):10–22.
795 72. Sofroniew MV. Molecular dissection of reactive astrogliosis and glial scar
796 formation. *Trends Neurosci*. 2009;32(12):638–647.
797 73. Patel S, Player MR. Colony-stimulating factor-1 receptor inhibitors for the
798 treatment of cancer and inflammatory disease. *Current topics in medicinal*
799 *chemistry*. 2009;9:599-610.
800 74. Li J, Chen K, Zhu L, Pollard JW. Conditional deletion of the colony stimulating
801 factor-1 receptor (c-fms proto-oncogene) in mice. *Genesis*. 2006;44:328-335.
802 75. Fabene PF, et al. A role for leukocyte-endothelial adhesion mechanisms in
803 epilepsy. *Nature medicine*. 2008;14:1377-1383.
804 76. Zattoni M, et al. Brain infiltration of leukocytes contributes to the
805 pathophysiology of temporal lobe epilepsy. *The Journal of neuroscience*.
806 2011;31:4037-4050.
807 77. Xu D, et al. Peripherally derived T regulatory and γδ T cells have opposing
808 roles in the pathogenesis of intractable pediatric epilepsy. *The Journal of*

experimental medicine. 2018;215:1169-1186.

78. Imura Y, et al. Microglia release ATP by exocytosis. *Glia*. 2013;61(8):1320–1330.

79. Shigetomi E, Hirayama YJ, Ikenaka K, Tanaka KF, Koizumi S. Role of purinergic receptor P2Y1 in spatiotemporal Ca(2+) dynamics in astrocytes. *J Neurosci*. 2018;38(6):1383–1395.

Figure legends

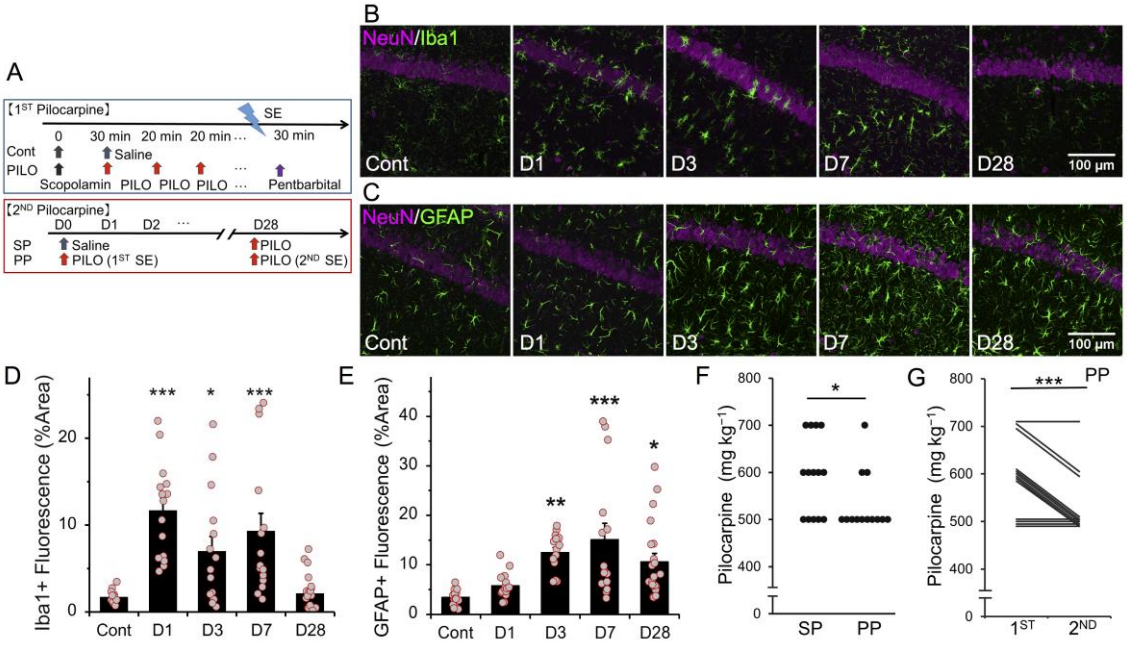

Fig 1. Astrogliosis is observed following microglial activation after SE.

(A) As shown in the experimental protocols, mice were administered pilocarpine to achieve stage 5 seizures. The second SE was induced using the same protocol 4 weeks after the first SE. SP (PP) indicates that mice were injected with saline (pilocarpine) at 8 weeks of age followed by an injection of pilocarpine at 12 weeks of age. (B and C) Representative microphotographs showing the spatiotemporal characteristics of Iba-1 (B) or GFAP (C) expression in CA1 after SE. Fifteen images were captured per z-stack image (0.5 μm step). Cont, control; D, day. (D and E) Quantification of the temporal profile of Iba-1 positive microglia (D) or GFAP positive astrocytes (E) after SE (n = 5 mice (D); n = 5, 5,

5, 5, 7 mice, (E), *P < 0.05, **P < 0.01 vs. control, one-way ANOVA (P < 0.001) with Dunnett's test). (F) Dot plots showing dose of pilocarpine required for the induction of the second SE (n = 14, 13 mice, *P < 0.05, Mann–Whitney U-test). (G) Scatter plot showing dose of pilocarpine required for the induction of the first (at 8 weeks of age) and second (at 12 weeks of age) SE in the PP group (n = 13 mice, **P < 0.01, Wilcoxon signed-rank test). Values represent the mean ± SEM.

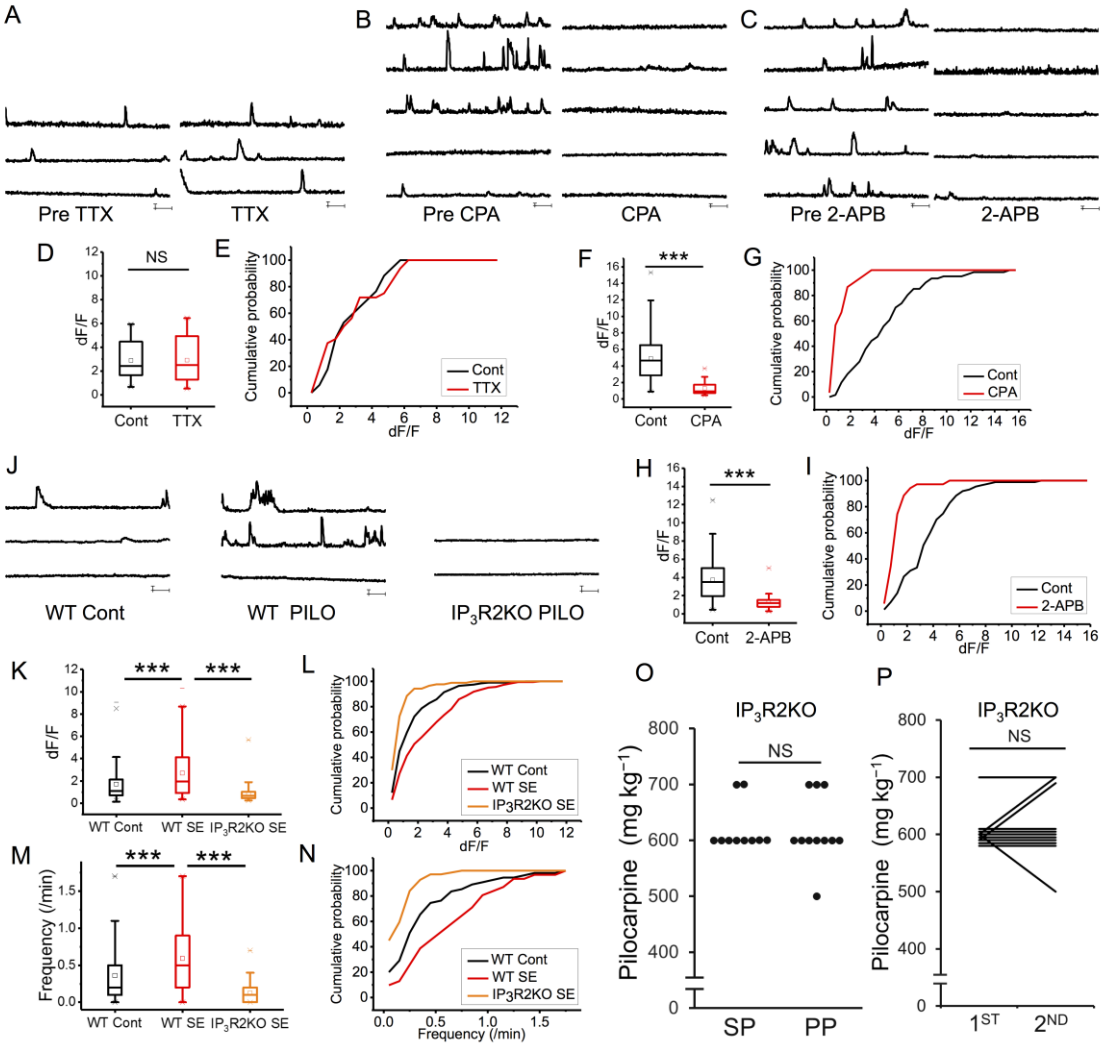

Fig 2. Reactive astrocytes exhibit IP_3R2-mediated Ca^{2+} hyperactivity, which is essential for epileptogenesis.

(A-C) Ca^{2+} dynamics of astrocytes approximately 4 weeks after SE in the CA1 stratum radiatum region in Glast-CreERT2::flx-GCaMP3 mice before and after TTX (1 μM) (A), CPA (20 μM) (B), and 2-APB (100 μM) (C) application. (D-I) Box plots showing amplitudes of Ca^{2+} signals before and after TTX (1 μM) (D), CPA (20 μM) (F), and 2-APB (100 μM) (H) application. (n = 10, 13, 14 cells/2

843 mice, ***P < 0.001, unpaired t-test). Cont, control. Cumulative probability plots
844 showing amplitudes (dF/F) of Ca^{2+} signals before and after TTX (not significant
845 (P > 0.05), Kolmogorov–Smirnov test) (E), CPA (P < 0.001, Kolmogorov–
846 Smirnov test) (G), and 2-APB (P < 0.001, Kolmogorov–Smirnov test) (**I**)
847 application. (J) Astrocytic Ca^{2+} dynamics by Fluo4 in the CA1 stratum radiatum
848 region in WT control, WT after SE, and IP_3R2KO mice after SE. (K-N) Box plots
849 showing Ca^{2+} signal amplitudes (dF/F) (K) and frequency (M) (n = 57, 32, 85
850 cells/2, 2, 3 mice, ***P < 0.001, unpaired t-test). Cumulative probability plots
851 showing Ca^{2+} signal amplitudes (dF/F) (L) and frequency (N) (P < 0.001,
852 Kolmogorov–Smirnov test). (O) Dot plots showing dose of pilocarpine required
853 for the induction of the second SE in IP_3R2KO mice. SP (PP) indicates mice
854 were injected with saline (pilocarpine) at 8 weeks of age followed by an injection
855 of pilocarpine at 12 weeks of age. (n = 10 mice, N.S., not significant (P > 0.05),
856 Mann–Whitney U-test). (P) Scatter plot showing dose of pilocarpine required for
857 the induction of the first (at 8 weeks of age) and second (at 12 weeks of age)
858 SE in the PP group regarding IP3R2KO mice (n = 10 mice, N.S., not significant
859 (P > 0.05), Wilcoxon signed-rank test). Note: The first pilocarpine did not affect
860 the dose required for the second SE in IP_3R2KO, see Fig 1G.

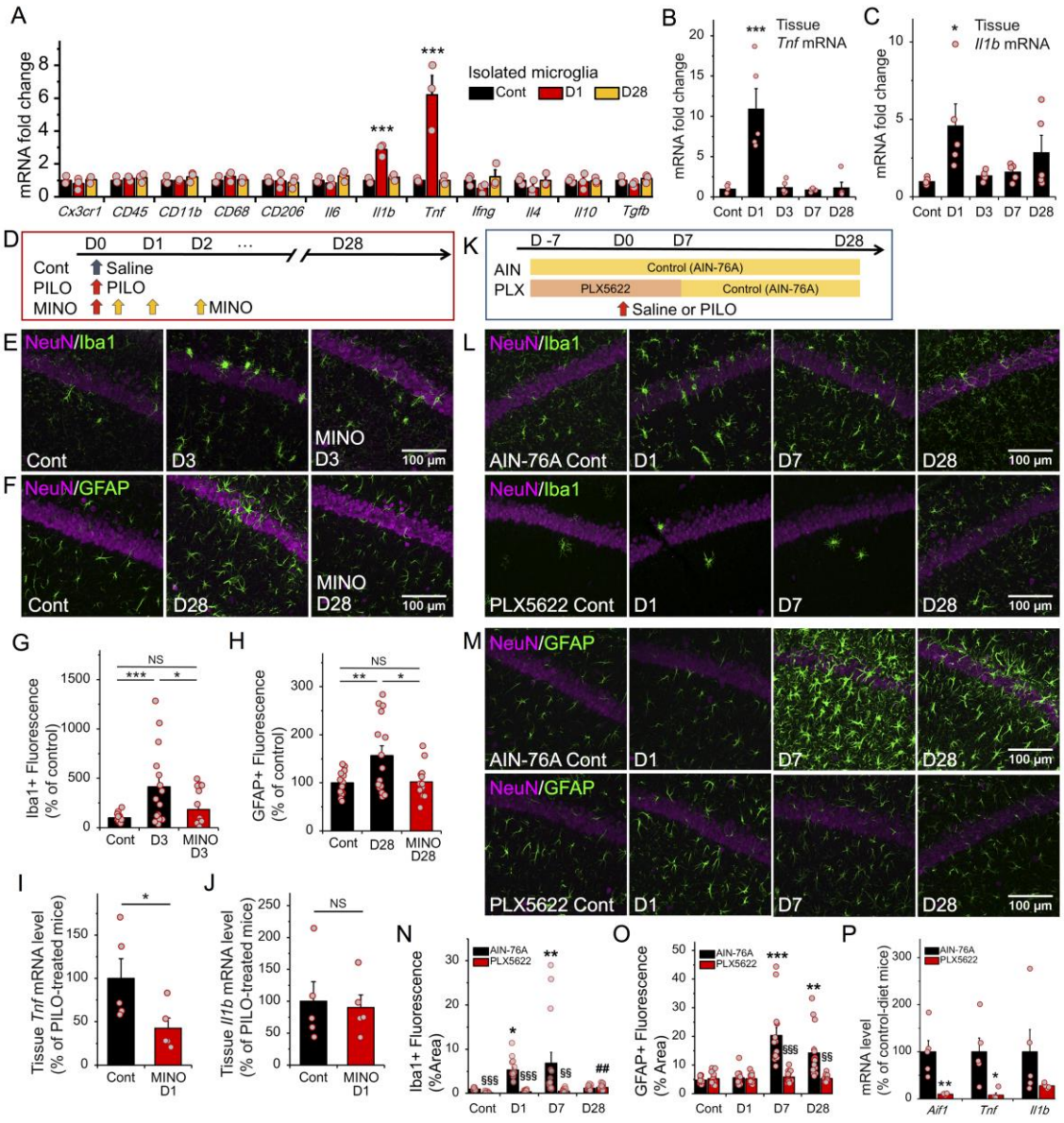

Fig 3. Microglia inhibition with minocycline and depletion with CSF1R antagonist (PLX5622) reduces astrogliosis.

(A) Microfluidic quantitative RT-PCR analysis of mRNA in total RNA extracted from hippocampal microglia after SE (n = 3 samples/9 mice, ***P < 0.001 vs. control, one-way ANOVA (P < 0.01, P < 0.001) with Dunnett's test). (B and C)

867 Quantitative RT-PCR analysis of mRNA in total hippocampal RNA after SE (n =
868 5 mice, *P < 0.05, ***P < 0.001 vs. control, one-way ANOVA (P < 0.001, P <
869 0.05) with Dunnett's test). (D) Experimental scheme for minocycline post-
870 treatment-mediated microglia inhibition. (E-H) Representative microphotographs
871 showing the spatiotemporal characteristics of Iba-1 (E) and GFAP (F)
872 expression and quantification of Iba-1 positive microglia (G) and GFAP positive
873 astrocytes (H) in CA1 with or without minocycline post-treatment after SE (n = 5
874 mice, N.S., not significant (P > 0.05), *P < 0.05, ***P < 0.001, one-way ANOVA
875 (P < 0.01) with Bonferroni test). (I and J) Quantitative RT-PCR analysis as in (B
876 and C) with or without minocycline post-treatment. (n = 5 mice, N.S., not
877 significant (P > 0.05), *P < 0.05, unpaired t-test). (K) Experimental scheme for
878 PLX5622-mediated microglia depletion. (L-O) Representative microphotographs
879 showing the spatiotemporal characteristics of Iba-1 (L) and GFAP (M)
880 expression and quantification of Iba-1 positive microglia (N) and GFAP positive
881 astrocytes (O) in CA1 with or without PLX5622 after SE (n = 5 mice, *P < 0.05,
882 **P < 0.01 vs. control of AIN-76A (control diet), $^{\#\#}P$ < 0.01 vs. control of
883 PLX5622, $^{\S}P$ < 0.05, $^{\S\S}P$ < 0.01, $^{\S\S\S}P$ < 0.001 vs. AIN-76A (corresponding day),
884 one-way ANOVA (P < 0.01) with Dunnett's test and unpaired t-test). (P)

885 Quantitative RT-PCR analysis as in (B and C) with or without PLX5622. (n = 5

886 mice, *P < 0.05, **P < 0.01, unpaired t-test).

887

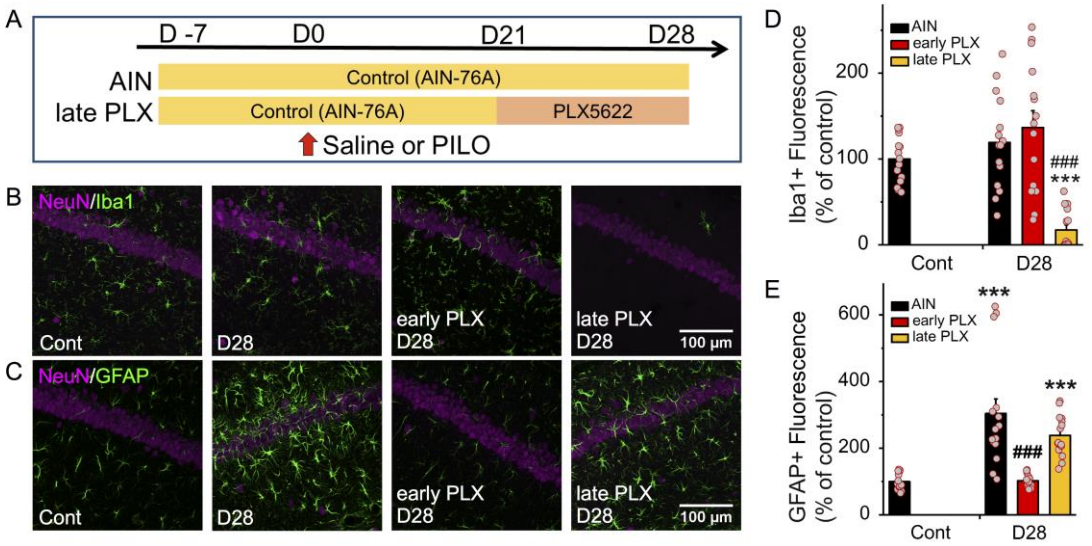

888

889 **Fig 4. Microglia depletion with CSF1R antagonist (PLX5622) at late phase**

890 **after SE does not reduce astrogliosis and increased seizure susceptibility.**

891 (A) Experimental scheme for microglia depletion with PLX5622 at the late phase

892 after SE. (B and C) Representative microphotographs showing the

893 spatiotemporal feature of Iba-1 (B) and GFAP (C) expression in CA1 with or

894 without PLX5622 after SE. Fifteen images were collected per z-stack image (0.5

895 μm step). Cont, control; D, day. (D and E) Quantification of the temporal profile

896 of Iba-1 positive microglia (D) and GFAP positive astrocytes (E) after SE (n = 5

897 mice, ***P < 0.01 vs. control, unpaired t-test, $^{###}P$ < 0.01 vs. AIN-76A

898 (corresponding day), one-way ANOVA (P < 0.001) with Dunnett's test). Values

899 represent the mean ± SEM.

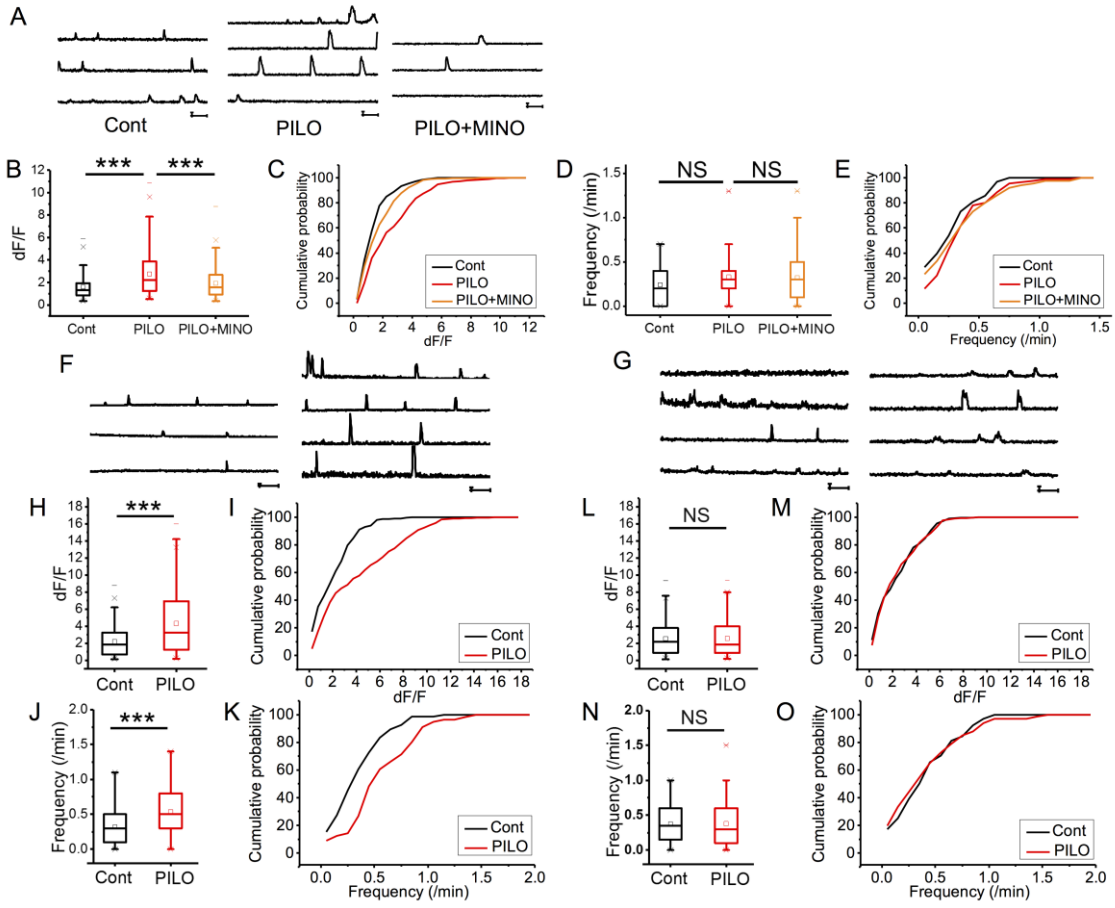

Fig 5. Microglia inhibition with minocycline or CSF1R antagonist (PLX5622) reduces the increased astrocytic Ca^{2+} hyperactivity following SE.

(A) Ca^{2+} dynamics of astrocytes approximately 4 weeks after SE in the CA1 stratum radiatum region in Glast-CreERT2::flx-GCaMP3 mice with or without minocycline treatment. (B-E) Box plots showing Ca^{2+} signal amplitude (dF/F) (B) and frequency (D) (n = 74, 92, 93 cells/3 mice, N.S., not significant ($P > 0.05$), ***$P < 0.001$, unpaired t-test). Cumulative probability plots showing Ca^{2+} signal amplitude (dF/F) ($P < 0.001$, Kolmogorov–Smirnov test) (C) and frequency (not

significant ($P > 0.05$), Kolmogorov–Smirnov test) (E). (F and G) Ca^{2+} dynamics of astrocytes approximately 4 weeks after SE in the CA1 stratum radiatum region in Glast-CreERT2::flx-GCaMP3 mice with (G) or without (F) PLX5622 treatment. (H-K) Box plots showing Ca^{2+} signal amplitude (dF/F) (H) and frequency (J) in the AIN-76A (control diet) group. (n = 70, 58 cells/2 mice, ***$P < 0.001$, unpaired t-test). Cumulative probability plots showing Ca^{2+} signal amplitude (dF/F) ($P < 0.001$, Kolmogorov–Smirnov test) (I) and frequency ($P < 0.001$, Kolmogorov–Smirnov test) (K) in the AIN-76A (control diet) group. (L-O) Box plots showing Ca^{2+} signal amplitude (dF/F) (L) and frequency (M) in the PLX5622 group. (n = 61, 71 cells/2 mice, N.S., not significant ($P > 0.05$), unpaired t-test). Cumulative probability plots showing Ca^{2+} signal amplitude (dF/F) (not significant ($P > 0.05$), Kolmogorov–Smirnov test) (M) and frequency (not significant ($P > 0.05$), Kolmogorov–Smirnov test) (O) in the PLX5622 group.

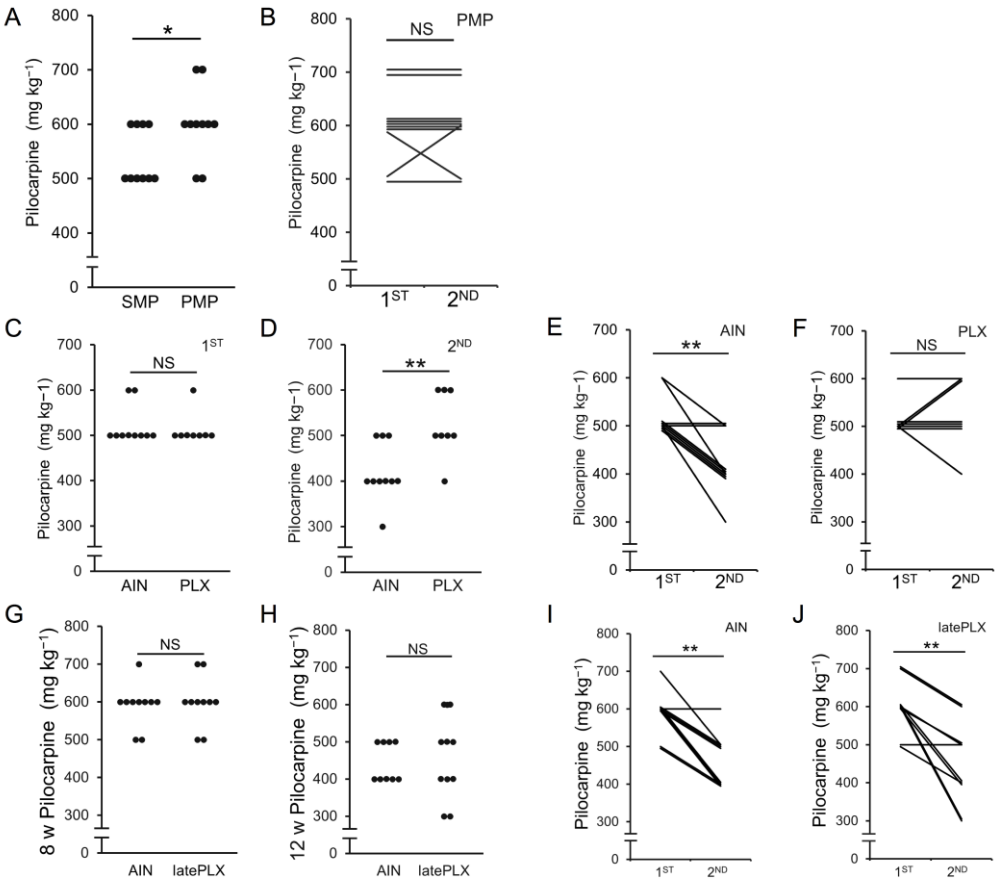

Fig 6. Microglia inhibition with minocycline or CSF1R antagonist (PLX5622) reduces the increased seizure susceptibility following SE.

(A) Dot plots showing dose of pilocarpine required for the induction of the second SE (n = 10 mice, N.S., not significant ($P > 0.05$), *$P < 0.05$, Tie-collected Mann–Whitney U-test). SMP (PMP) indicates that mice were injected with saline (pilocarpine) at 8 weeks of age with minocycline post-treatment followed by an injection of pilocarpine at 12 weeks of age. (B) Scatter plot showing dose of pilocarpine required for the induction of the first (at 8 weeks of age) and second

(at 12 weeks of age) SE. (n = 10 mice, **P < 0.01, Wilcoxon signed-rank test). (C and D) Dot plots showing dose of pilocarpine required for the induction of the first (C) and second (D) SE with or without PLX5622. (n = 10, 8 mice, N.S., not significant (P > 0.05), **P < 0.01, Mann–Whitney U-test). AIN, control diet (AIN-76A). (E and F) Scatter plot showing dose of pilocarpine required for the induction of the first (at 8 weeks of age) and second (at 12 weeks of age) SE for AIN-76A (control diet) (E) or PLX5622 (F). (n = 10, 8 mice, N.S., not significant (P > 0.05), **P < 0.01, Wilcoxon signed-rank test). (G and H) Dot plots showing dose of pilocarpine required for the induction of the first (G) and second (H) SE with or without late PLX5622 treatment. (n = 10 mice, N.S., not significant (P > 0.05), Mann–Whitney U-test). (I and J) Scatter plot showing dose of pilocarpine required for the induction of the first (at 8 weeks of age) and second (at 12 weeks of age) SE AIN-76A (control diet) (I) or PLX5622 (J). (n = 10 mice, **P < 0.01, Wilcoxon signed-rank test).

Supporting Information

S1 Fig Microglia depletion with CSF1R antagonist (PLX5622) or IP_3R2KO mice reduces the increased interictal spikes following SE.

S2 Fig Initial microglial activation is observed after SE in IP3R2KO mice.

S3 Fig Immunohistochemical analysis of GCaMP expression in the hippocampus in Glast-CreERT2::Flx-GCaMP3 mice.

S1 Table Cell-specific markers in GCaMP3-expressing cells in the hippocampus of Glast-CreERT2::Flx-GCaMP3 mice (tamoxifen i.p. at P7).

S1 Movie Astrocytic Ca^{2+} dynamics revealed by Fluo4 in the CA1 stratum radiatum region in WT control, WT after SE, and IP_3R2KO mice after SE.

S2 Movie Ca^{2+} dynamics of astrocytes approximately 4 weeks after SE in the CA1 stratum radiatum region in Glast-CreERT2::flx-GCaMP3 mice before and after TTX application.

S3 Movie Ca^{2+} dynamics of astrocytes approximately 4 weeks after SE in the CA1 stratum radiatum region in Glast-CreERT2::flx-GCaMP3 mice before and after CPA application.

S4 Movie Ca^{2+} dynamics of astrocytes approximately 4 weeks after SE in the CA1 stratum radiatum region in Glast-CreERT2::flx-GCaMP3 mice before and

after 2-APB application.

S5 Movie Ca^{2+} dynamics of astrocytes in the CA1 stratum radiatum region in Glast-CreERT2::flx-GCaMP3 control mice, and approximately 4 weeks after SE, with or without minocycline treatment.

S6 Movie Ca^{2+} dynamics of astrocytes approximately 4 weeks after SE in the CA1 stratum radiatum region in Glast-CreERT2::flx-GCaMP3 mice.

S7 Movie Ca^{2+} dynamics of astrocytes approximately 4 weeks after SE in the CA1 stratum radiatum region in Glast-CreERT2::flx-GCaMP3, mice with or without PLX5622 treatment.

Supporting information

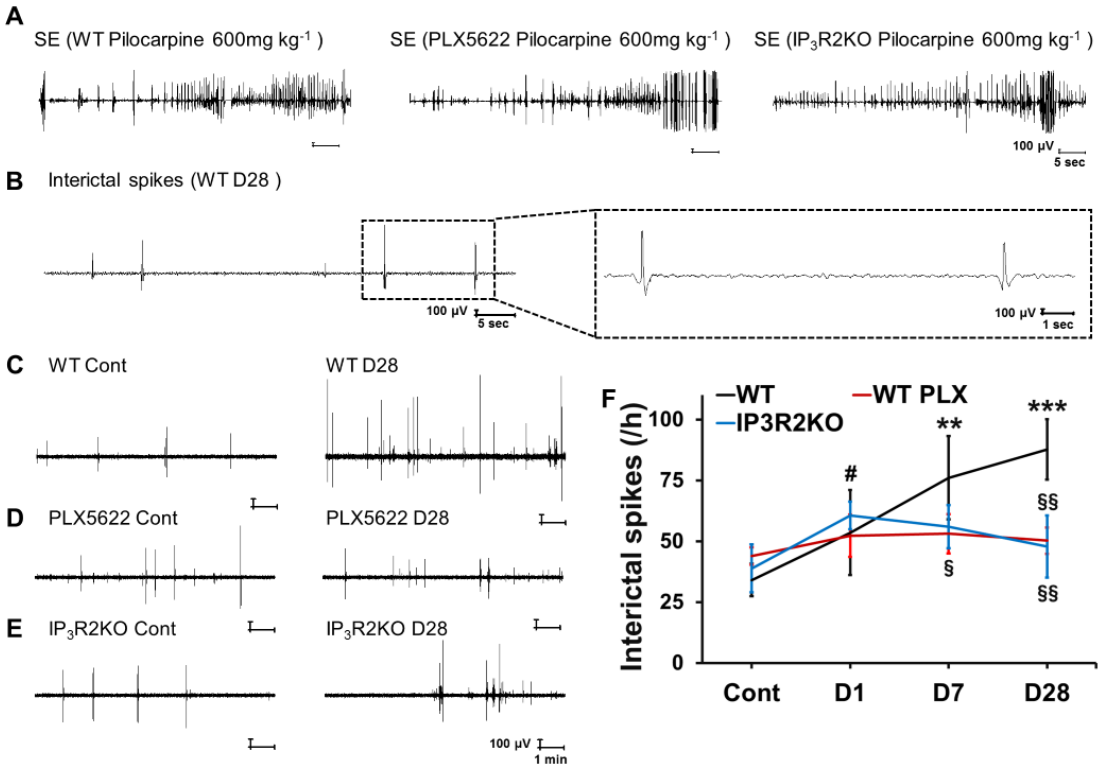

S1 Fig Microglia depletion with CSF1R antagonist (PLX5622) or IP$_3$R2KO mice reduces the increased interictal spikes following SE.

(A) Sample EEG from a WT, PLX5622-treated and IP$_3$R2 knockout mouse during a pilocarpine-induced stage 5 seizure. (B) Sample EEG presenting Interictal spikes from a WT mouse at 28 days after SE. (C) Interictal spikes (for 10 min) in WT control and 28 days after SE. (D) Interictal spikes (for 10 min) in WT control and 28 days after SE with PLX5622 treatment. (E) Interictal spikes (for 10 min) in IP$_3$R2KO mice control and 28 days after SE. (F) Quantification of the temporal profile of interictal spikes after SE (n = 5 mice, $^{**}P < 0.01$, $^{***}P < 0.001$ vs. control

of WT mice, $^{\#}P < 0.05$ vs. control of PLX5622, $^{\S}P < 0.05$, $^{\S\S}P < 0.01$ vs. WT (corresponding day), one-way ANOVA ($P < 0.01$) with Dunnett's test and unpaired t-test). Values represent the means ± SEM. Cont, control; D, day.

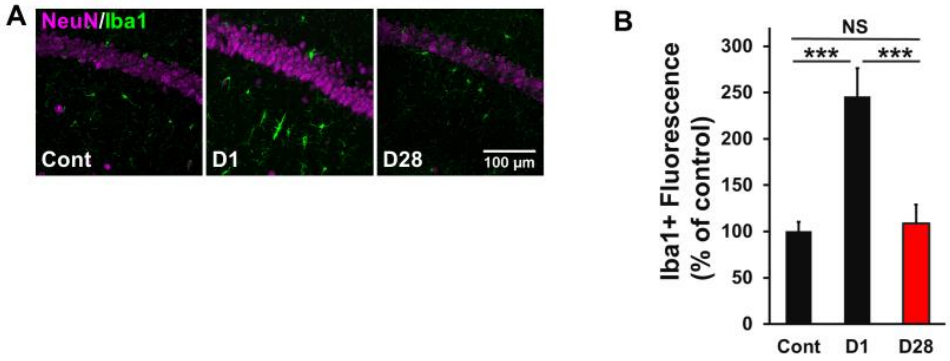

990

991 **S2 Fig Initial microglial activation is observed after SE in IP$_3$R2KO mice.**

992 (A) Representative microphotographs showing the spatiotemporal characteristics

993 of Iba-1 expression in CA1 after SE. Fifteen images were captured per z-stack

994 image (0.5 μm step). (B) Quantification of the temporal profile of Iba-1 positive

995 microglia in IP$_3$R2KO mice after SE (n = 4 mice, N.S. means not significant (P >

996 0.05), ***P < 0.001, one-way ANOVA (P < 0.001) with Bonferroni test). Values

997 represent the mean ± SEM. Cont, control; D, day.

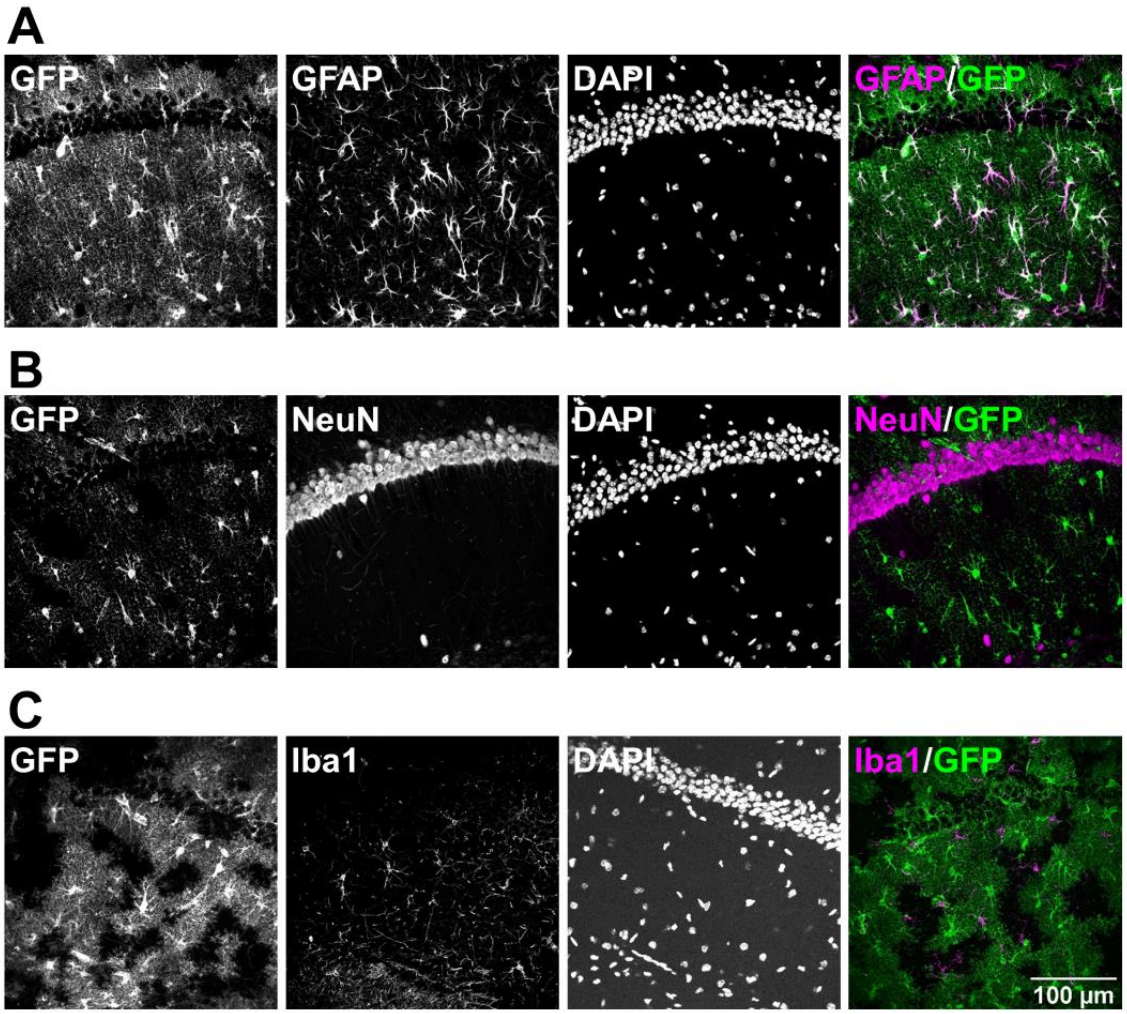

998

999 **S3 Fig Immunohistochemical analysis of GCaMP expression in the**

1000 **hippocampus in Glast-CreERT2::Flx-GCaMP3 mice.**

1001 (A to C) Representative images showing immunohistochemical staining for GFAP

1002 (A), NeuN (B), and Iba1 (C) with GFP staining in the CA1 region of Glast-

1003 CreERT2::Flx-GCaMP3 mice (tamoxifen i.p. at P7).

S1 Table Cell-specific markers in GCaMP3-expressing cells in the hippocampus of Glast-CreERT2::Flx-GCaMP3 mice (tamoxifen i.p. at P7).

Region	GFAP/GFP	NeuN/GFP	Iba1/GFP
CA1	92 ± 2% (12 FOV/6 slices)	0 ± 0% (12 FOV/6 slices)	0 ± 0% (12 FOV/6 slices)
CA2	86 ± 5% (6 FOV/6 slices)	0 ± 0% (6 FOV/6 slices)	0 ± 0% (6 FOV/6 slices)

n = 3 mice, values represent the means ± SEM. FOV, fields of view.